Chapter 5

Design of Starch-Based Electro-Responsive Smart Hydrogel with Rapid Bending Actuation Under Low-Electric Field

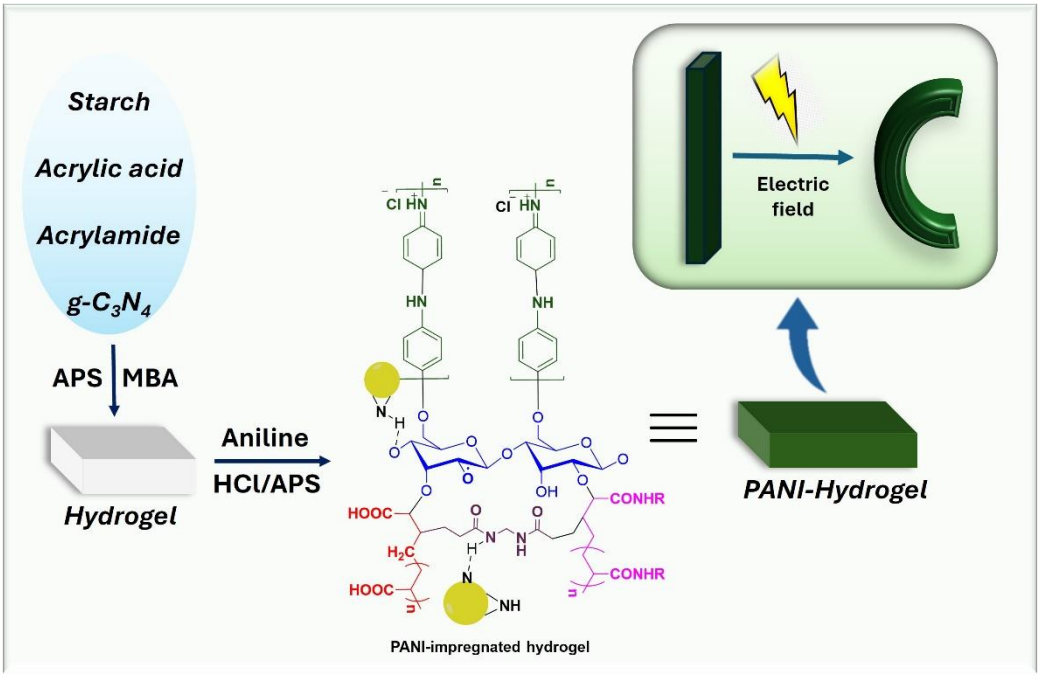

This chapter demonstrates an electrically responsive hydrogel synthesized by integrating conductive polyaniline (PANI) with a polyelectrolyte-based hydrogel. The resulting hydrogel demonstrates enhanced electrical properties and exhibits repeatable actuation in response to cyclic electric fields. Moreover, the mechanical strength of the hydrogel has been improved by incorporating g-C_3N_4 into the hydrogel matrix.

5.1 Introduction

As already discussed in Chapter 1, smart hydrogels have emerged in recent decades as promising materials for numerous applications, including drug delivery [1,2], tissue engineering [3], sensors [4], actuators [5], etc. These hydrogels are highly sensitive to external stimuli, and even a small change in their external environment such as light, heat, electric field, pressure, or pH can alter their physical or chemical properties [6-10]. The changes that occur are mostly reversible. Hydrogel actuators are smart hydrogels that undergo reversible expansion or contraction under such stimuli [11]. In particular, hydrogel actuators that respond to electric fields and convert electric energy into mechanical energy have gained widespread attention because of their fast actuation and low energy requirement. They can be easily and remotely controlled by varying the applied electric fields. Moreover, hydrogel actuators, with their high water content, flexibility, biocompatibility, and good mechanical strength, bring a revolutionary change in various applications such as soft robotics [12], artificial muscle [13], prosthetic devices [14], etc. Most hydrogel actuators are based on polyelectrolyte hydrogels that contain ionizable groups in their network structures. When placed in an electrolyte solution, they show mechanical responses when the electric field is applied [15-17]. Numerous studies have been done in synthesizing polyelectrolyte-based hydrogel actuators. Generally, synthetic hydrogels containing polyelectrolytes with ionic groups, such as 2-acrylamido-2-methylpropane sulphonic acid (AMPS), have been used for synthesizing hydrogel actuators. However, the challenge is to synthesize hydrogel with biocompatibility, and biodegradability. Therefore, it is necessary to utilize natural polymers, such as starch, gelatin, chitosan, etc., in synthesizing hydrogel actuators. Starch is an abundant naturally derived carbohydrate found widely in plant sources. It is formed by amylose and amylopectin connected by (1,4) and (1,6) linkage. Starch-based hydrogels found applications in many electrochemical devices, including electrical double-layer capacitors (EDLC) or supercapacitors [18], in flexible electronics [19,20], as a polymer electrolyte in supercapacitors [21,22], etc.

The responsive behavior of hydrogel actuators is based on many factors, such as the ionic strength of the electrolyte, the applied electric field, and the distance between the electrodes and the hydrogel [23,24]. Although much research has been done on synthesizing polyelectrolyte-based hydrogel, most require high electric voltage for large mechanical changes. For example, Jiang and coworkers developed electric field

responsive actuators by fabricating acrylic acid (AAc) and *N,N*-dimethyl acrylamide (DMAA), using aluminum hydroxide nanoparticles (AH NPs) as multi-functional crosslinkers. The maximum bending deviation was around 55° with an applied electric field of 15 V [25]. In another work, Rotjanasuworapong and his coworkers developed an agarose-based hydrogel, and their electro-responsive properties are studied under various conditions. They examined the bending response of the hydrogel as a function of electric field strength in the range of 0-600 V, and the highest deflection was around 70° [26]. Similarly, Li and his coworkers synthesized negatively charged hydrogel using 2-acrylamido-2-methylpropane sulphonic acid hydrogel using F127DA micelles as crosslinkers. The hydrogel shows a high compressive strength of 59 MPa. The electro-responsive behavior of the hydrogel was studied using an electrolyte. Under an applied electric field of 20 V, the hydrogel showed a maximum bending of 80° [27]. Therefore, to improve the electro-responsive properties of hydrogel actuators, conductive polymers such as polyaniline (PANI), polypyrrole (PPy), and poly-(3,4-ethylenedioxythiophene) (PEDOT) are incorporated for faster mechanical deformation. They create a continuous electron conduction network due to the π-electron's delocalization in their conjugated system [28]. Lin *et al*. demonstrate the increased conductive property of a hydrogel by incorporating a conductive polymer through their study. They synthesized a conductive hydrogel of polyacrylate/polyaniline (PAAc/PANI) and poly(2-acrylamido-2-methyl propylsulfonic acid-acrylic acid)/polyaniline [P(AMPS-AAc)/PANI] and determined their electro-responsive bending behavior under an applied voltage of 25 V. They found that by increasing the aniline dosage, electro-responsive behavior also increases [29]. Operating hydrogel actuators under a high electric field restricts their applications in many areas. Therefore, it is necessary to develop hydrogels that operate under low electric fields as they possess advantages such as biocompatibility, safety, low energy consumption, and ease of fabrication.

In this chapter, we have developed a starch-based electric-field responsive hydrogel by using polyelectrolyte AMPS and AAc using ammonium persulphate (APS) as an initiator and *N,N′*-methylenebisacrylamide (MBA) as a crosslinker. Hydrogel formed by using AMPS exhibits excessive swelling, leading to the formation of a mechanically weak and brittle hydrogel. Therefore, graphitic carbon nitride (g-C_3N_4) has been used as a reinforcer to give soft hydrogel and at the same time maintain the mechanical strength of the hydrogel. The formed hydrogel is then incorporated with polyaniline to improve

the electric-field responsive property of the hydrogel. To investigate the feasibility of the synthesized hydrogel as an actuator, a series of bending experiments have been performed, and the effect of varied electric fields, electrolyte concentration, and hydrogel thickness on the rate of bending actuation has been evaluated. The swelling behavior of the hydrogel at varied ionic strength is also determined. In addition, the effect of the reinforcing agent on the hydrogel's mechanical properties is determined by performing tensile and compression tests on the hydrogel.

5.2 Experimental Section

5.2.1 Materials

Acrylic acid (AAc), 2-Acrylamido-2-methyl-1-propanesulphonic acid (AMPS), and *N*,*N*′-methylenebis(acrylamide) (MBA) were purchased from Sigma Aldrich. Ammonium peroxodisulfate (APS) and Polyaniline were obtained from Merck. Starch was purchased from Qualigens. Deionized water was used during the experiment for preparing various solutions. All the reagents used were of analytical grade and were used as received.

5.2.2 Synthetic procedures

5.2.2.1 Synthesis of hydrogel

The hydrogel is synthesized using the thermally induced free-radical polymerization method. Initially, a fixed amount of starch is dissolved in 5ml water at 70 °C for about 2 hr. AAc and AMPS are added to the solution, followed by the addition of the crosslinker. In another vessel, bulk g-C_3N_4 was dispersed under ultrasonication for an hour and was added to the above solution. The reaction was initiated using free radical initiator APS. The reaction mixture was flushed with N_2 atmosphere for 30 mins and was kept stirring until a thick gel was formed. The formed gel was washed with distilled water several times and kept for further studies. (The detailed compositions of the precursors are shown in Table 1)

5.2.2.2 Impregnation of PANI into the hydrogel matrix

The as-prepared hydrogel was soaked into an aqueous solution of 0.25 M APS and 1 M HCl for PANI impregnation for 24 h. After that, the hydrogel was removed from the solution and again immersed in a hexane solution containing 0.2 M aniline for 2 hours. The temperature was maintained at 0-5 °C. Aniline was absorbed into the

hydrogel matrix, leading to contact with the oxidative medium resulting in the formation of PANI after polymerization. The conducting composite hydrogel was dipped into 1 M HCl aqueous solution for 2 days to wash out low molecular components and the unreacted APS and PANI oligomers.

Table 5.1 Detailed compositions of the precursors used in the formation of hydrogels

Starch (g)	*AMPS (g)*	*AAc (ml)*	*g-C_3N_4 (wt%)*	*PANI*	*Hydrogel*
0.5	0.6	0.5	1	✓	SAA-gCN-1
0.5	0.6	0.5	1.2	✓	SAA-gCN-1.2
0.5	0.6	0.5	2	✓	SAA-gCN-2
0.5	0.6	0.5	1	✓	SAA-gCN-1
0.5	0.6	0.5	1	×	SAA-gCN-1-NP
0.5	0.6	0.5	0		SAA-gCN-0

5.3 Characterization

The chemical structure of the synthesized hydrogels is characterized by using Fourier Transform Infrared Spectroscopy (FTIR). The FTIR spectra of the hydrogels and the monomers were recorded using Impact 410 (Nicolet, USA) FTIR spectrometer within the range of 4000-400 cm^{-1}, and the number of scans was four. The morphology of the synthesized hydrogel at various conditions was analyzed using a Scanning Electron Microscope (SEM, Model-JSM-6390 LV, JEOL, Japan) coupled with an Energy-dispersive X-ray detector to determine the elemental composition of the synthesized hydrogel. The thermal stability of the hydrogel is analyzed using a Shimadzu TA-60 thermogravimetric analyzer with a heating rate of 10°C/min under N_2 atmosphere and up to a maximum temperature of 600 °C. The powder X-ray diffraction (XRD) data were recorded in the range of 2θ= 10°-80° using a Rigaku Miniflex X-ray diffractometer (Tokyo, Japan) by employing Cu Kα radiation (λ= 0.1548 nm) at a voltage of 30 kV and 15 mA current.

5.3.1 Determination of swelling behavior of the hydrogel

The prepared hydrogel samples were dried to a constant weight. The dried samples with varied compositions were then immersed in pure water and electrolyte solutions of

different ionic strengths. The hydrogel samples were taken out at a certain interval, soaked up the excess water, and weighed. The weight of the hydrogel samples was measured until an equilibrium was reached. The swelling percentage of the hydrogel is calculated using the formula:

$$\text{Swelling } \% = \frac{W_s - W_d}{W_d} \times 100$$

W_s and W_d are the weights of the swollen and dehydrated samples respectively.

5.3.2 Mechanical Tests

The mechanical strength of the hydrogel is determined by performing both the tensile and compressive tests on the hydrogel sample using a Universal Tensile Machine (UTM, Zwick, Z010, ASTM D638). The tensile tests are carried out by stretching a thin strip of the as-prepared hydrogel sample until the break with a constant loading rate of 100 mm/min. The tensile tests were carried out on different samples with varied compositions.

Similarly, the compressive strength of the hydrogel was also determined. For the test, a thick slab of the hydrogel sample is compressed to a fixed strain, and its compressive strength is measured. The hydrogel sample was compressed for up to 20 cycles with an interval of 10 min between each cycle.

5.3.3 Bending actuation under electric field

A transparent chamber containing two carbon electrodes 40 mm apart, filled with NaCl aqueous solution was taken for the bending actuation experiment. The as-prepared hydrogel was swelled in the desired electrolyte solution before the experiment. Then a thin strip is cut from the swelled hydrogel, fixed at one end, and placed vertically between the two electrodes. The hydrogel strip starts to bend when a voltage is applied using a DC power source (name). This bending actuation is recorded using a digital camera. The experiment was analyzed by varying the thickness of the hydrogel strip, ionic strength, and applied voltage. The degree of deviation of the hydrogel from its original location is calculated and is known as the bending angle. The equipment used for the experiment is illustrated in Figure 5.1

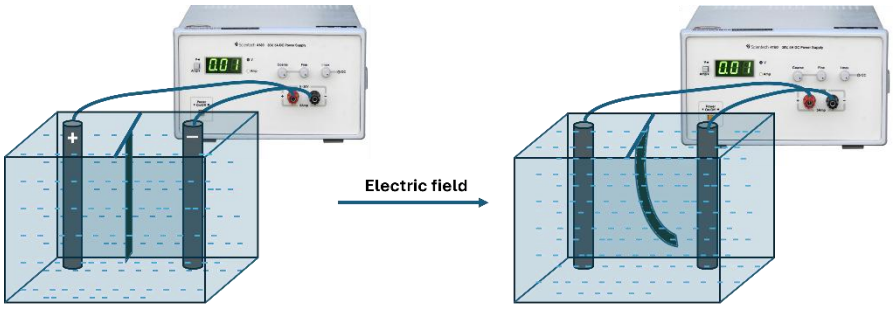

Figure 5.1 Schematic diagram showing the electrodes dipped in an electrolyte solution connected to a DC power source with a strip of hydrogel placed in between the electrodes

5.4 Results and Discussion

5.4.1 Fabrication strategy of the hydrogel

The synthetic procedure for fabricating an electroactive hydrogel proceeds through two major steps. In the first step, the synthesis of copolymer hydrogel takes place. All the precursors, such as starch, AMPS, and AAc, were dissolved in water in a round-bottomed flask. The MBA as a crosslinker, along with dispersed g-C_3N_4, are also added to the above solution. The reaction proceeds in an inert atmosphere through a free radical polymerization process where APS acts as a thermal initiator. Here, on heating, the APS produces sulfate ($\cdot SO_4$) radical, which then reacts with water to form hydroxyl ($\cdot OH$) radical. These free radicals then initiate the precursor molecule, followed by propagation of the polymeric chain, and finally crosslinked to give the white-colored polymeric hydrogel.

In the second step, PANI impregnation into the hydrogel matrix occurs. Here, the hydrogel matrix is first activated by immersing it in a solution of APS and HCl. After aniline is added to the hydrogel, it undergoes *in situ* polymerization to form polyaniline (PANI). Aniline undergoes protonation and is grafted to the hydrogel matrix *via* free radical polymerization. This results in the change of hydrogel's color from white to dark green, which is the typical color of PANI. The plausible mechanism involved in the formation of hydrogel is shown in Scheme 5.1 and its schematic diagram is shown in Figure 5.2

Step 1: Synthesis of copolymer hydrogel

Step 1a: Formation of Sulphate radicals

$$(NH_4)_2S_2O_8 \xrightarrow{\triangle} 2NH_4^+ + S_2O_8^{2-}$$

$$S_2O_8^{2-} \xrightarrow{\triangle} 2\dot{S}O_4^-$$

$$\dot{S}O_4^- + H_2O \xrightarrow{\triangle} HSO_4^- + OH^-$$

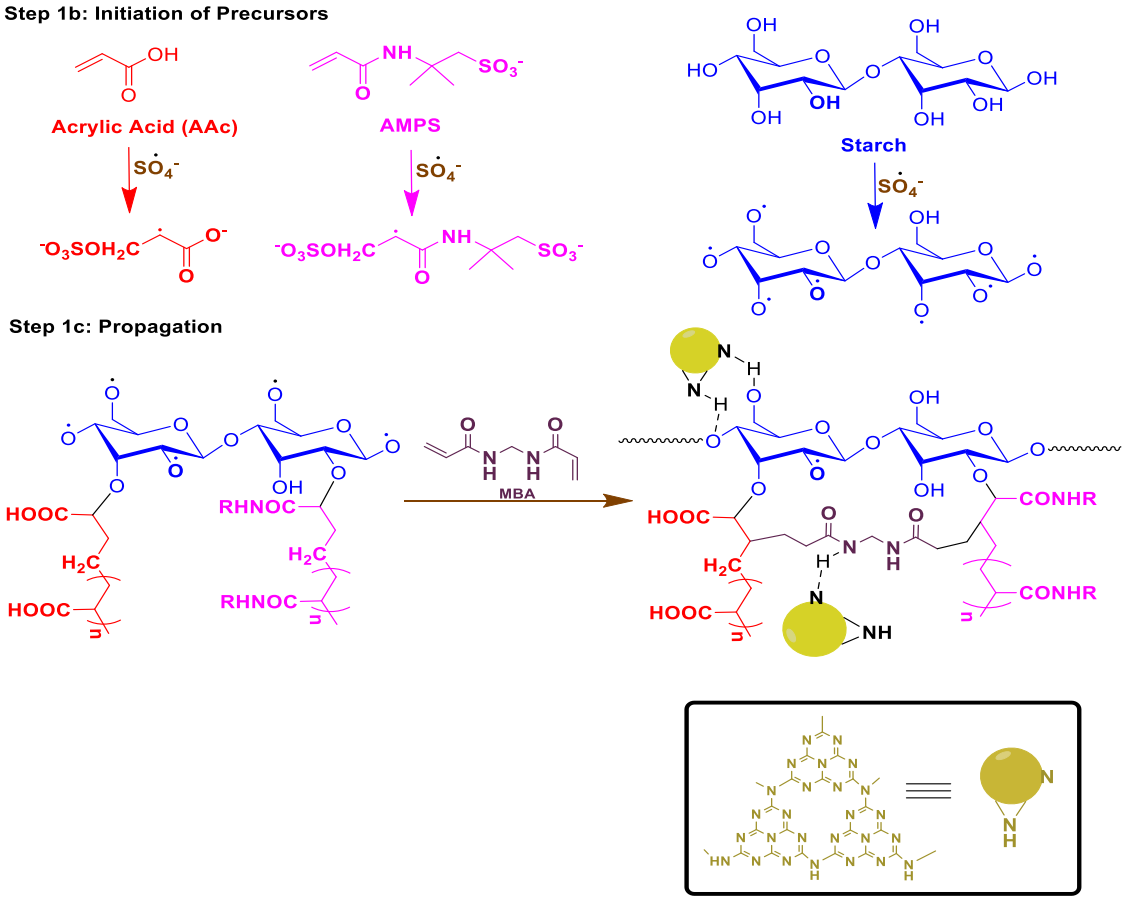

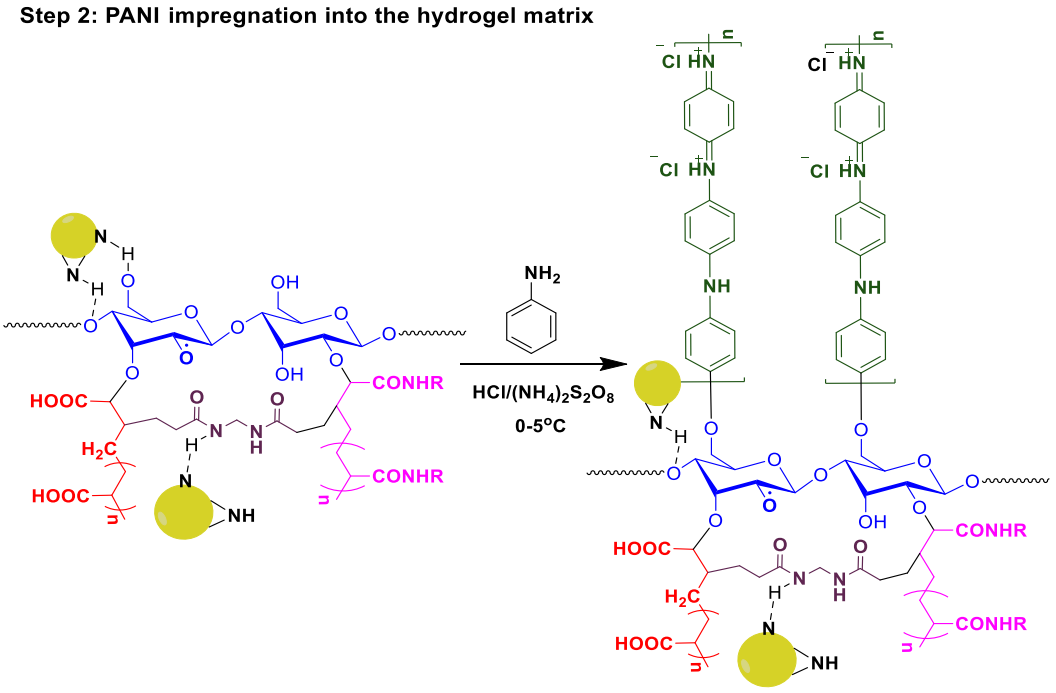

Scheme 5.1 Plausible mechanism involved in the formation of hydrogel

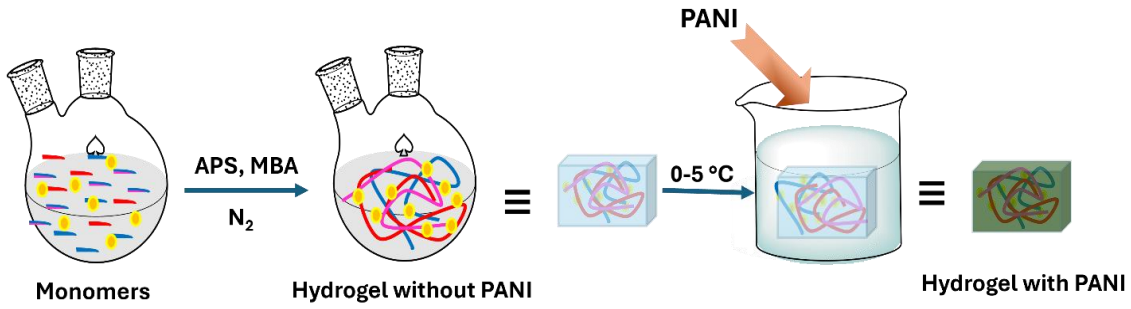

Figure 5.2 Schematic diagram showing hydrogel formation

5.4.2 Characterization of the hydrogel by FTIR spectral analysis

The FTIR spectra of the monomers and hydrogel are shown in Figure 4. From Figure 5.3(a), it is seen that the AMPS monomer showed a broad peak at around 3400 cm^{-1} which can be attributed to the overlapping of stretching frequency of OH (SO_3H) and $–NH_2$ groups. The peak at 2987 cm^{-1} is due to the C–H stretching of the $–CH_2$ group. Again, the two peaks at 1668 cm^{-1} and 1662 cm^{-1} are due to the C=O stretching frequency of the amide I band and N-H bending of the amide II band. The peak at 1379 cm^{-1} appears due to asymmetric stretching of the S=O bond and the peaks at 1079 cm^{-1} and 975 cm^{-1} depict the stretching frequency of the S–O–C group. The peak at 628 cm^{-1} is due to C-S absorption. Similarly, for the AAc monomer, the broad peak around 3458 cm^{-1} is due to the stretching frequency of the –OH group and the peaks at 1726 cm^{-1} and 1622 cm^{-1} are due to the stretching frequency of C=O and C=C respectively. Again, the peak at 984 cm^{-1} can be attributed to the deformational vibration of the –OH group. The FTIR spectra for native starch showed a broad peak around 3300 cm^{-1} which can be attributed to the stretching frequency of the –OH groups. The peaks at 1158 cm^{-1} and 1015 cm^{-1} are due to the C–O stretching frequency of the ether and alcohol groups respectively. The multiple peaks from 853 cm^{-1} to 570 cm^{-1} appear due to the anhydro glucose ring stretching vibrations.

The spectrum of the hydrogel (SAA-gCN-2) as shown in Figure 5.3(b) displayed the characteristic peak of the precursors used. Many peaks, that appeared in the spectra of the precursors have been diminished in the spectra of the hydrogel and many peaks appear to be sharp in the spectra of the hydrogel due to the formation of a cross-linked structure. Sharp peaks at 2927 cm^{-1} and 2851 cm^{-1} occur due to the stretching frequency of the C–H bond in the methylene groups depicting the saturation of the C=C bond after polymerization. Again, the peaks in the range of 1600 cm^{-1}-1700 cm^{-1} in spectra of the

precursors overlapped in the hydrogel's spectra and gave a new peak at 1633 cm^{-1} and a shoulder at 1718 cm^{-1} indicating C=O vibrations. Again, a peak at 1431 cm^{-1} indicates the presence of C=C of the aromatic ring depicting the presence of polyaniline in the hydrogel matrix. Thus, the significant occurrence of new peaks and shifting of old peaks depicts the formation of a crosslinked network structure thereby indicating the formation of a hydrogel.

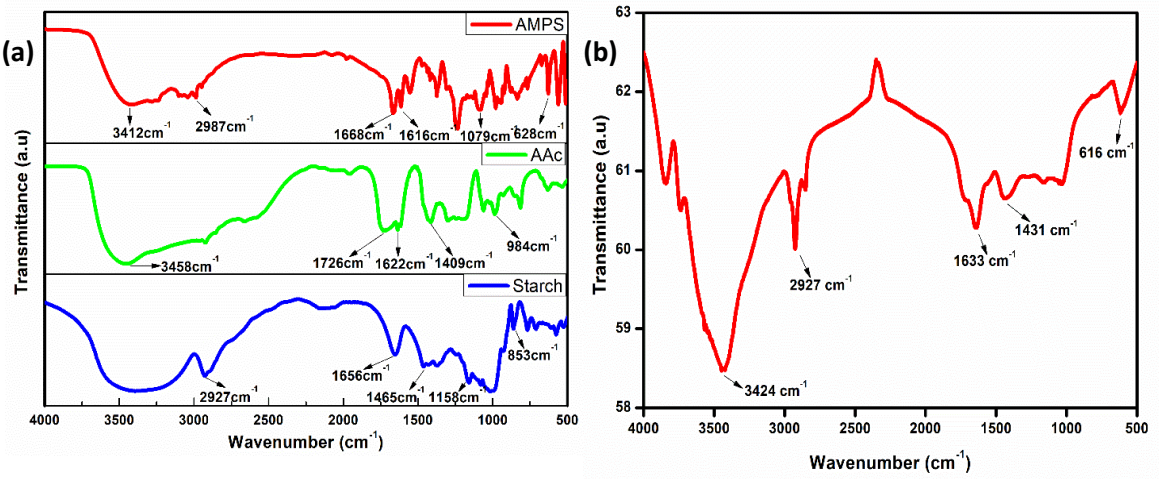

Figure 5.3 FTIR spectra of (a) precursors and (b) SAA-gCN-2 hydrogel

5.4.3 Morphological and elemental analysis of the hydrogel

The morphology of the synthesized hydrogel has been studied through SEM analysis. The SEM image of the hydrogel at various conditions is shown in Figure 5.4. Hydrogel without g-C_3N_4 (SAA-gCN-0) showed homogenously dispersed spherical structures. The spherical structures are due to the presence of PANI in the hydrogel matrix. (Figure 5.4 (a)) However, the incorporation of g-C_3N_4 (SAA-gCN-2) brings non-uniformity to the surface of the hydrogel with the formation of clusters of g-C_3N_4 in the surface as shown in Figure 5.4 (b)

The energy-dispersive X-ray spectroscopy reveals that the hydrogel PAA-gCN-0 exhibits the weight percentage ratio of C, N, O, and S to be 49.69:6.02:34.40:9.88. However, on adding g-C_3N_4, the hydrogel PAA-gCN-2 exhibits a percentage weight ratio of 40:10.69:41.72:7.58. This increase in the weight percentage of N and decrease in C reveals the successful incorporation of g-C_3N_4 into the hydrogel matrix. The elemental analysis spectra of the hydrogels are shown in Figure 5.4(c) and (d).

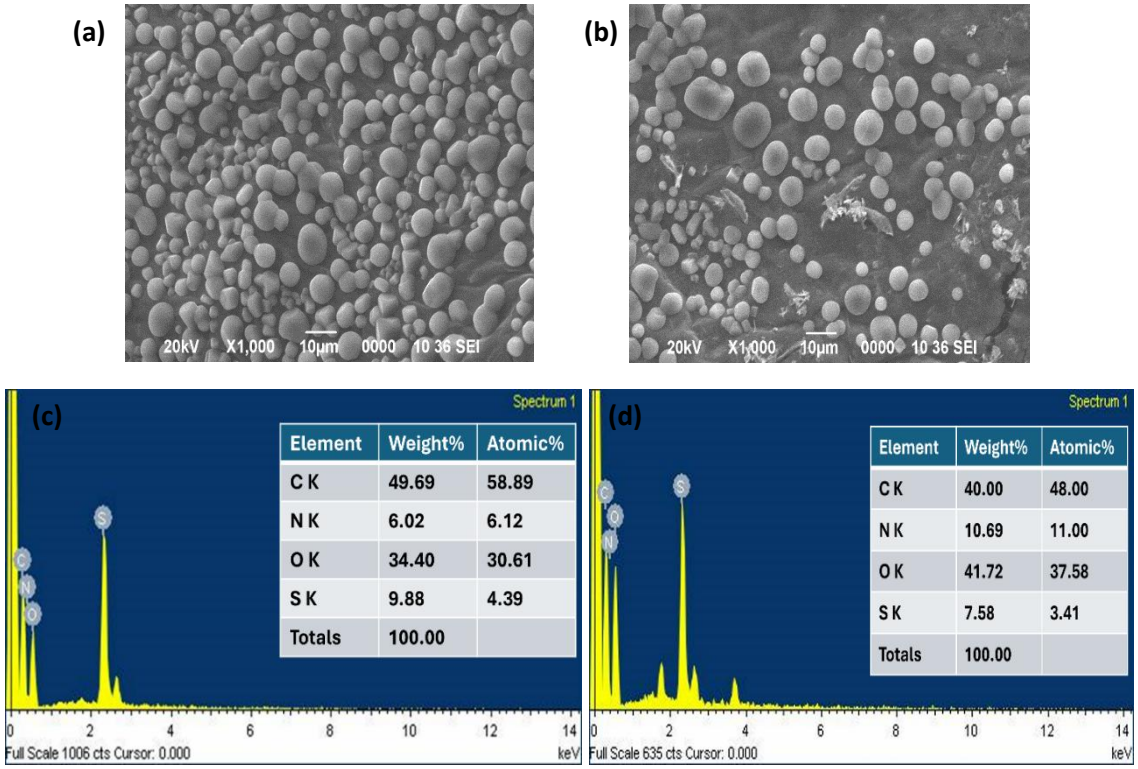

Figure 5.4 SEM image of (a) SAA-gCN-0 and (b) SAA-gCN-2; EDX of (c) SAA-gCN-0 and (d) SAA-gCN-2

5.4.4 Thermal study of the hydrogel using TGA

Again, comparing the TGA spectra of the two hydrogels, PAA-gCN-0 and PAA-gCN-2, shows a slight difference in their weight loss behavior. The PAA-gCN-2 hydrogel showed weight loss at an elevated temperature compared to the PAA-gCN-0 hydrogel. This is because of the crosslinking effect of g-C_3N_4 on the hydrogel matrix. The initial weight loss of around 9% is probably due to the loss of moisture content within the hydrogel matrix. Further, a decrease in weight up to 330 °C can be attributed to the degradation of the functional groups within the hydrogel network. Finally, on increasing the temperature above 350 °C, the breaking of the C-C bond takes place, leading to the degradation of the polymeric chain. Therefore, results from the TGA spectra reveal that hydrogel is stable and can be applied in various applications under a wide range of temperatures up to 100 °C. The TGA spectra of the hydrogels are shown in Figure 5.5

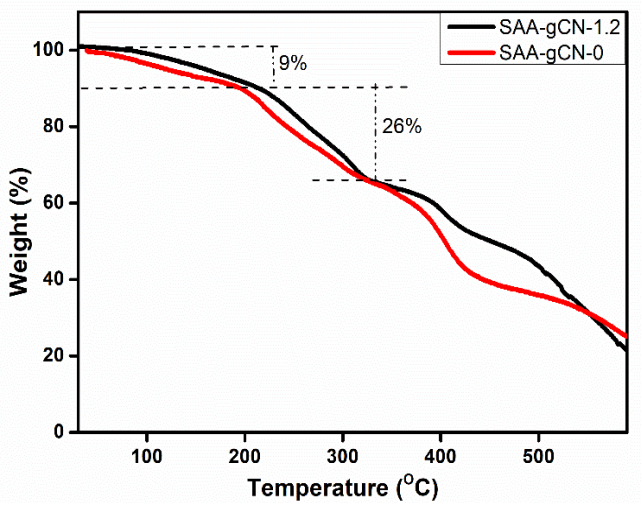

Figure 5.5 TGA spectra of the hydrogels with and without g-C_3N_4

5.4.5 Swelling behavior of the hydrogel

The swelling behavior of the hydrogel is an important property in determining its nature and strength for various applications. Here, swelling behavior is examined at different time intervals by considering other parameters such as electrolyte concentration and cross-linking density. Figure 5.6(a) shows the swelling behavior of PAA-gCN-2 hydrogel in pure water and at the different ionic strengths of NaCl. It is found that the swelling of the hydrogel in pure water is 1150 % within 1 h and it gradually increases with time and reaches a swelling of 4258 % within 48 h. This excellent swelling is due to the hydrophilic functional groups such as –COOH, –SO_3H, and –NH– present in their network structure that form hydrogen bonding with water molecules. In addition, the electrostatic repulsion among the charged group also enhances the polymer chain to extend, thereby causing further swelling of the hydrogel. However, on placing the hydrogel in an electrolyte solution of various ionic strengths such as 0.01, 0.015, 0.02, and 0.025, the swelling of the hydrogel decreases compared to its swelling in water. This can be attributed to the presence of ions such as Na^+ and Cl^- in the solution which interfere with the hydrogen bonding between the water molecules and the hydrogel. In addition, the shielding effect caused by the ions in the solutions on the fixed charge in the hydrogel network reduces the swelling capability of the hydrogel. Again, comparing the swelling of the hydrogel at different concentrations of electrolytes reveals a slight increase in their swelling percentage with an increase in electrolyte concentrations. The fixed charges on the hydrogel network attract the counterion in the solution leading to the osmotic pressure difference in the solutions and within the hydrogel. This causes diffusion of water into the hydrogel to balance the pressure resulting in swelling of the

hydrogel. However, with a small increase in the ion concentrations in the solution, more ions will be attracted into the hydrogel until saturation of the charged groups, leading to an increased swelling [30,31].

Again, the swelling of the hydrogel with and without PANI incorporation in an electrolyte solution of 0.01 N ionic strength is also evaluated. (Figure 5.6(b)) The hydrogel without PANI shows a maximum swelling of 518.5 % after 1 h. However, on continuing further, the hydrogel shows a slight increase in swelling and rises to 566.6 in 48 h. On the other hand, the PANI-incorporated hydrogel shows swelling of 878.5 % after 1 h and reached a maximum swelling of 2071 % after 48 h. This tremendous increase in swelling on PANI incorporation is due to adding hydrophilic amine and imine groups present in PANI to the hydrogel matrix, which increases water absorbency.

Moreover, Figure 5.6(c) shows that by increasing the content of g-C_3N_4, the swelling of the hydrogel increases. The hydrogel with a g-C_3N_4 content of 0.4 wt% shows a maximum swelling of 485 %. On increasing the g-C_3N_4 content to 1 wt% and 2 wt%, their swelling increases to 1170 % and 1228 % respectively. This is due to the increased formation of new hydrogen bonding between the N atom of g-C_3N_4 and the water molecule which results in higher water uptake.

Thus, the above results showed that both g-C_3N_4 and PANI greatly impact the hydrogel's swelling behavior.

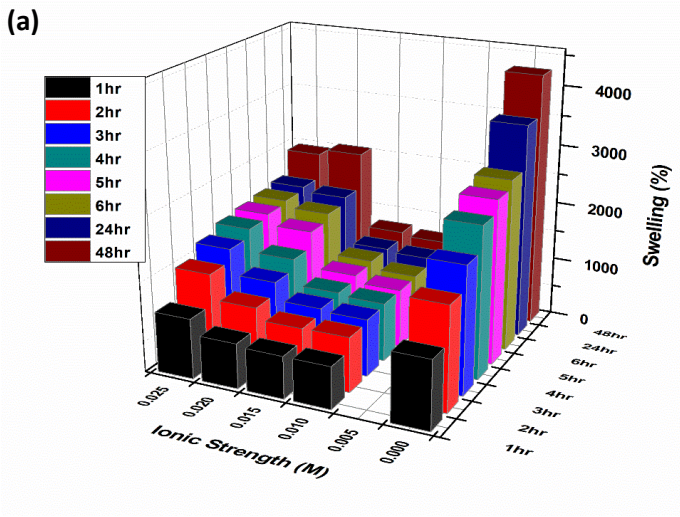

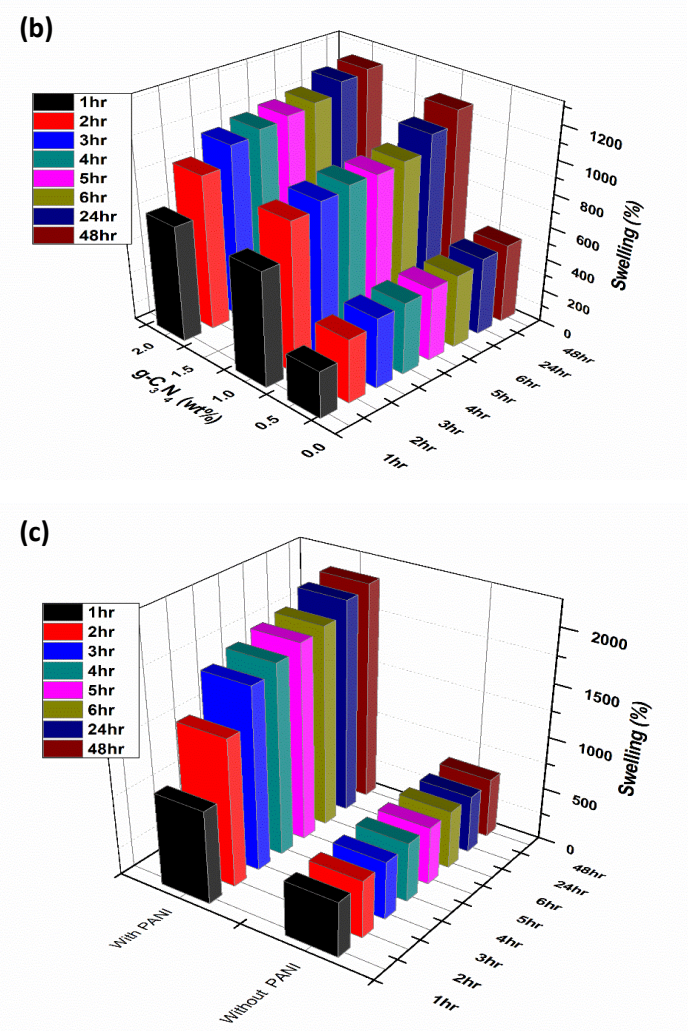

Figure 5.6 Swelling behavior of hydrogels with time as a function of (a) different ionic strength of NaCl, (b) PANI content, and (c) g-C_3N_4 content

5.4.6 Mechanical strength

The mechanical strength of the hydrogel is determined by performing tensile and compression tests on the hydrogel at various conditions. The tensile strength of the hydrogel with and without g-C_3N_4 is shown in Figure 5.7(a). The hydrogel without g-C_3N_4 (SAA-gCN-0) shows a tensile strength of 0.398 MPa with a strain of 81%. However, hydrogels with g-C_3N_4 (SAA-gCN-2) show a tensile strength of 0.96 MPa with a strain of 139%. The superior mechanical strength of the hydrogel containing g-C_3N_4 is due to the reinforcing effect of g-C_3N_4 on the hydrogel matrix. In addition, the impact of different contents of g-C_3N_4 on the mechanical strength of the hydrogel matrix is also studied. It was found that by increasing the content of g-C_3N_4 from 1 wt% to 2wt%, the tensile strength of the hydrogel shows a slight decrease in its value. However, the tensile strain of the hydrogel increases rapidly as shown in Figure 5.7(b). Again,

elastic modulus increases when g-C_3N_4 is added. This showed that adding g-C_3N_4 makes the hydrogel more elastic. However, after achieving a critical point, elastic modulus decreases by increasing the content of g-C_3N_4. This can be attributed to the additional crosslinking on the hydrogel matrix by incorporating more g-C_3N_4 which restricts the movement of the network structure within the hydrogel. Again, the toughness value confirms that g-C_3N_4 improves the mechanical strength of the hydrogel (Figure 5.7 (c) and (d).

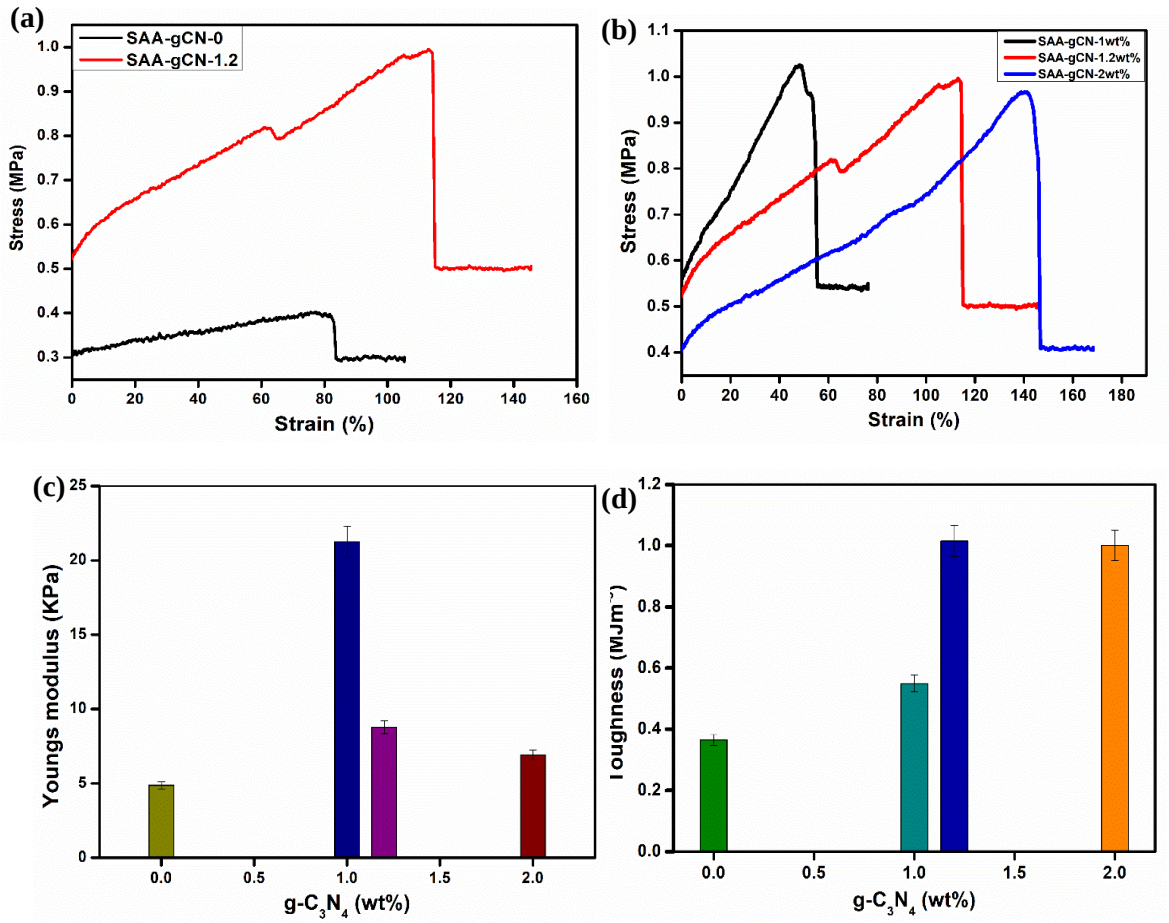

Figure 5.7 Tensile strength of hydrogels (a) without g-C_3N_4 (SAA-gCN-0) and with g-C_3N_4 (SAA-gCN-1.2) hydrogels, (b) with varied content of g-C_3N_4, (c) Young's modulus and (d) toughness of the hydrogel at varied content of g-C_3N_4

The compressive strength of the PAA-gCN-1 hydrogel and its repeatable compression are determined, as illustrated in Figure 5.8. From the figure, it is found that the hydrogel has a maximum compressive stress of 14.79 KPa. Repeating the compression on the hydrogel with an interval of 10 min shows no decline in strength even upon its 20th cycle. This reveals that synthesized hydrogel can be easily used in soft robotics and as actuators without fearing breaks or damage under stress.

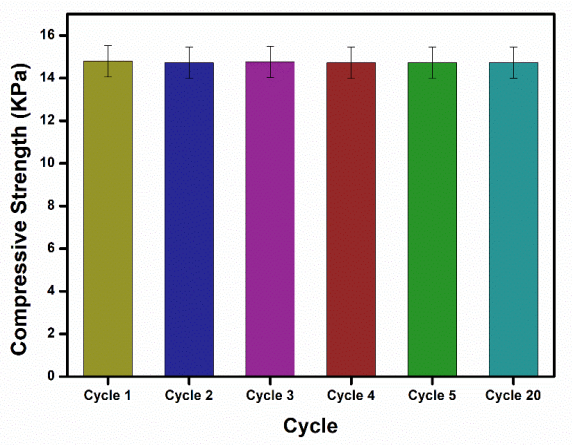

Figure 5.8 Cyclic compressive strength of SAA-gCN-1.2 hydrogel

5.5 Bending of hydrogel under low electric voltages

The hydrogel containing negatively charged groups shows bending when placed under an electric field in an electrolyte solution. The bending of the hydrogel strip is due to the osmotic pressure difference within the hydrogel matrix [32-35]. When an electric field is applied, the charged electrons start moving toward the counter electrodes. The movement of the negatively charged sulphonic and acrylic groups on the hydrogel network was restricted by the cross-linked structure of the hydrogel. However, their counterions inside the hydrogel and the free ions in the electrolyte solution keep moving towards their counter electrode. As a result, the ionic concentration on each side of the hydrogel varies causing an osmotic pressure difference. This leads to the bending of the hydrogel strip. The migration of the counter ions of the negatively charged sulphonic and acrylic groups towards the cathode causes higher osmotic pressure on the anode side than the osmotic pressure on the cathode side. Again, the fixed negatively charged ions on the hydrogel network and the mobile anions repel each other at the anode side causing easy penetration of the water molecule inside the hydrogel towards the anode side. Thus, the swelling of the hydrogel towards the anode and the shrinking of the hydrogel towards the cathode results in a rapid bending of the hydrogel towards the cathode

The electro-responsive behavior of the hydrogel towards electrical stimulation can be investigated by determining the bending actuation of the hydrogel under different reaction conditions. For this, a thin strip of hydrogel is placed between two electrodes connected to a power source and an electrolyte solution of NaCl. The bending actuation of the hydrogels is determined by capturing it in a camera and the variation in bending angle is measured. The variation in bending actuation of the hydrogel is determined by

varying the concentration of electrolytes, electric field strength, and thickness of the hydrogel strip.

5.5.1 Effect of ionic strength

The effect of the ionic strength of the electrolyte on the bending actuation of the hydrogel under an electric field of 9V is determined. The maximum bending actuation by the hydrogel at different concentrations of NaCl is shown in Figure 5.9(a). It was found that the maximum bending of the hydrogel at 0.01 N is 40° which increases to 60° on increasing the ionic strength to 0.015 N. On further increasing the ionic strength, the maximum bending angle decreases. This could be because, initially on increasing the ionic strength, the number of mobile ions increases. On reaching a critical value, the further increase in mobile ions shields the polyions on the hydrogel thereby decreasing the bending actuation. In addition, the rate of bending actuation as a function of the ionic strength of electrolytes is shown in Figure 5.9(b). The figure shows that, to a fixed angle of 40°, the rate of hydrogel bending increases initially and then decreases with an increase in electrolyte concentrations. The initial increase in the rate of bending actuation is again due to the increasing number of mobile ions in the surrounding medium. This causes rapid movement of the mobile ions to the hydrogel or the counter electrode. However, further increasing the concentration of electrolytes, the rapid increase in mobile ions causes a shielding effect to the polyions in the hydrogels. This results in the reduction of the response towards electrical stimuli thereby reducing the rate of bending actuation.

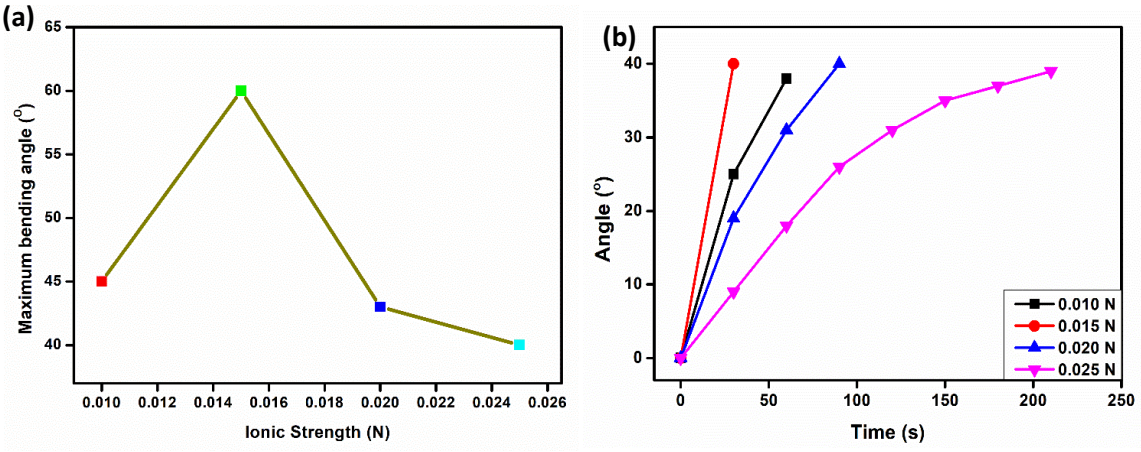

Figure 5.9 (a) Maximum bending angle as a function of ionic strength, (b) rate of bending actuation at varied ionic strength

5.5.2 Effect of electric field

The effect of electric field strength on the bending behavior of the hydrogel is also investigated. The bending actuation is carried out at an electrolyte concentration of 0.015 N. The hydrogel shows no bending when no electric field is applied and upon applying an electric voltage of 3 V, the hydrogel shows slight bending towards the cathode. However, increasing the voltage to 5 V and 7 V, the maximum bending angle rises to 20° and 30° respectively. Further increasing the voltage, the maximum bending angle rises rapidly to 60° at 9 V and 110° at 10 V. (Figure 5.10(a)). Similarly, the effect of applied voltage has been seen in the rate of bending actuation. The hydrogel is allowed to bend up to 20° and the rate of bending actuation is determined. Initially, with an applied electric field of 3 V and 5 V, the rate of bending actuation by the hydrogel is poor and keeps increasing with increasing applied voltage as shown in Figure 5.10(b). The rate of bending actuation is highest at 10V electric fields. This is simply because at higher voltage, the movement of mobile ions accelerates, and the ionization of the ionic groups becomes faster thereby causing the hydrogel to bend faster.

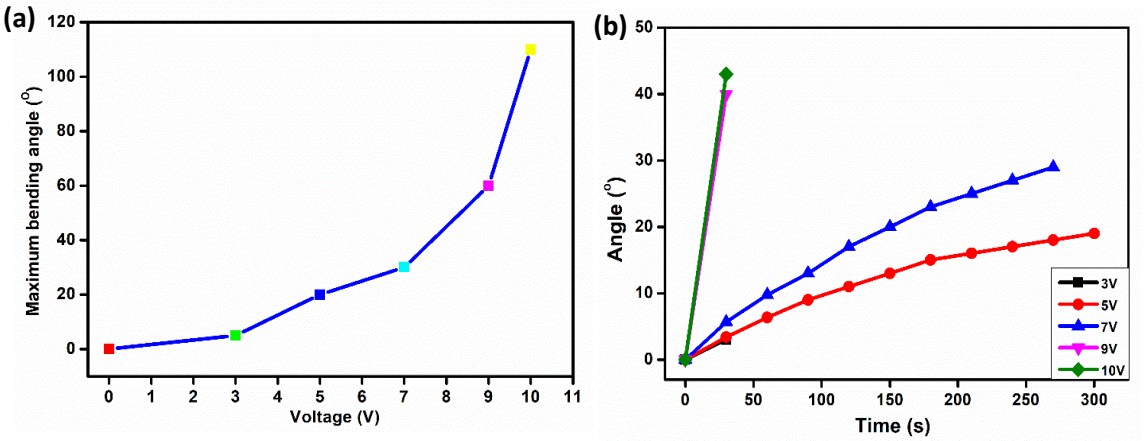

Figure 5.10 (a) Maximum bending angle as a function of electric field strength, (b) rate of bending actuation at an electric field of varied strength

5.5.3 Effect of thickness

Similarly, the thickness of the hydrogel material also affects its bending actuation. Figure 5.11 shows the rate of bending actuation by the hydrogel with different thickness values. It is seen that the rate of bending actuation decreases with increasing thickness of the hydrogel material. This is because the thicker the hydrogel is, the more pressure will be needed to bend the hydrogel than the pressure needed to bend a thin hydrogel. Additionally, thick hydrogel possesses more polyions in the hydrogel network causing them to move toward the anode which can also lower the bending actuation

toward the cathode. However, the rate of bending of hydrogel with a thickness of 0.5 mm is lower compared to hydrogel with 1 mm thickness. This can be attributed to the lower concentration of anionic groups in the former, causing less ionization and reducing the bending actuation rate.

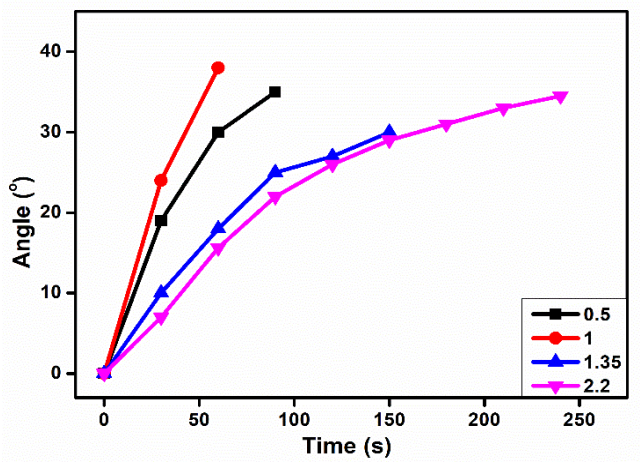

Figure 5.11. Rate of bending actuation at varied thickness

5.5.4 Cyclic bending actuation

The cyclic bending test of the hydrogel determines its ability to perform repetitive bending actuation. Under an applied voltage of 9 V, the hydrogel in 0.015 N NaCl showed repetitive bending behavior for up to 5 cycles with an interval of 10 min between each cycle. (Figure 5.14)

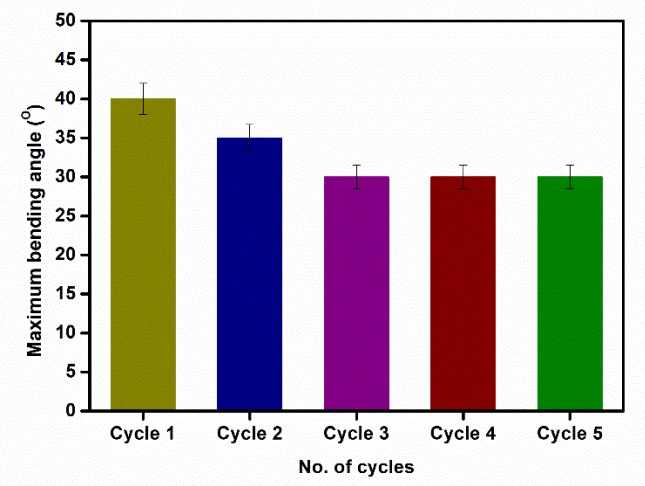

Figure 5.14. Repeatable bending actuation of the hydrogel on cyclically applying electric field

5.6 Conclusion

In conclusion, in this Chapter, we have successfully fabricated an electric field-responsive hydrogel by impregnating PANI as a conductive polymer into a

polyelectrolyte-based hydrogel. The effect of the electric field on the hydrogel was determined by performing bending actuation under different conditions. The highest bending deformation was achieved at 110° under an electric field strength of 10V with an electrolyte solution of ionic strength 0.015N. The PANI incorporation improves the conductivity of the hydrogel by promoting the charge transfer rate, thereby causing rapid electro-responsive behavior. This leads to a rapid bending deformation of the hydrogel and its swelling behavior. We also found that the bending behavior of the hydrogel is directly proportional to the thickness of the hydrogel strip used and the applied electric field strength. The mechanical strength of the hydrogel was also measured by performing tensile and compressive tests. The cyclic compression showed the flexibility of the synthesized hydrogel, and it was found that the incorporation of g-C_3N_4 could physically crosslink the polymeric chain and act as a reinforcing agent. This results in the effective transfer of load between the polymeric chain and g-C_3N_4, thereby improving the flexibility and mechanical strength of the hydrogel. The hydrogel also exhibits repeatable bending deformation by cyclically applying an electric field. Thus, the above findings indicate that the hydrogel can be remotely monitored, and the fast electro-responsive behavior reveals that the hydrogel has great potential to be applicable as an actuator and in soft robotics.

References

[1] Bordbar-Khiabani, A. and Gasik, M. Smart hydrogels for advanced drug delivery systems. *International Journal of Molecular Sciences*, 23(7):3665, 2022.

[2] Qu, J., Zhao, X., Ma, P.X. and Guo, B. Injectable antibacterial conductive hydrogels with dual response to an electric field and pH for localized “smart” drug release. *Acta biomaterialia*, 72:55-69, 2018.

[3] Khan, M.U.A., Stojanović, G.M., Abdullah, M.F.B., Dolatshahi-Pirouz, A., Marei, H.E., Ashammakhi, N. and Hasan, A.. Fundamental properties of smart hydrogels for tissue engineering applications: A review. *International Journal of Biological Macromolecules*, 254:127882, 2024.

[4] Li, J., Ding, Q., Wang, H., Wu, Z., Gui, X., Li, C., Hu, N., Tao, K. and Wu, J. Engineering smart composite hydrogels for wearable disease monitoring. *Nano-Micro Letters*, 15(1):105, 2023.

[5] Ko, H. and Javey, A. Smart actuators and adhesives for reconfigurable matter. *Accounts of chemical research*, 50(4):691-702, 2017.

[6] Kolosnjaj-Tabi, J., Gibot, L., Fourquaux, I., Golzio, M. and Rols, M.P.. Electric field-responsive nanoparticles and electric fields: physical, chemical, biological mechanisms and therapeutic prospects. *Advanced drug delivery reviews*, 138:56-67, 2019.

[7] Shinn, J., Kwon, N., Lee, S.A. and Lee, Y. Smart pH-responsive nanomedicines for disease therapy. *Journal of Pharmaceutical Investigation*, 52(4):427-441, 2022.

[8] Li, L., Scheiger, J.M. and Levkin, P.A. Design and applications of photoresponsive hydrogels. *Advanced Materials*, 31(26):1807333, 2019.

[9] Li, Z., Li, Y., Chen, C. and Cheng, Y. Magnetic-responsive hydrogels: From strategic design to biomedical applications. *Journal of Controlled Release*, 335:541-556, 2021.

[10] Marefat Seyedlar, R., Imani, M., Atai, M. and Nodehi, A. Temperature-Responsive Hydrogels: Materials, Mechanisms and Biological Applications. *Iranian Journal of Polymer Science and Technology*, 31(3):211-237, 2018.

[11] Shang, J., Le, X., Zhang, J., Chen, T. and Theato, P. Trends in polymeric shape memory hydrogels and hydrogel actuators. *Polymer Chemistry*, 10(9):1036-1055, 2019.

[12] Chen, Y., Zhang, Y., Li, H., Shen, J., Zhang, F., He, J., Lin, J., Wang, B., Niu, S., Han, Z. and Guo, Z. Bioinspired hydrogel actuator for soft robotics: Opportunity and challenges. *Nano Today*, 49:101764, 2023.

[13] Oveissi, F., Fletcher, D.F., Dehghani, F. and Naficy, S. Tough hydrogels for soft artificial muscles. *Materials & Design*, 203:109609, 2021.

[14] Cui, Y., Li, D., Gong, C. and Chang, C. Bioinspired shape memory hydrogel artificial muscles driven by solvents. *ACS nano*, 15(8):13712-13720, 2021.

[15] Shin, Y., Choi, M.Y., Choi, J., Na, J.H. and Kim, S.Y. Design of an electro-stimulated hydrogel actuator system with fast flexible folding deformation under a low electric field. *ACS Applied Materials & Interfaces*, 13(13):15633-15646, 2021.

[16] Mo, K., He, M., Cao, X. and Chang, C. Direct current electric field induced gradient hydrogel actuators with rapid thermo-responsive performance as soft manipulators. Journal of Materials Chemistry C, 8(8):2756-2763, 2020.

[17] Shi, Q., Liu, H., Tang, D., Li, Y., Li, X. and Xu, F. Bioactuators based on stimulus-responsive hydrogels and their emerging biomedical applications. *NPG Asia Materials*, 11(1):64, 2019.

[18] Jeżowski, P. and Kowalczewski, P.L. Starch as a green binder for the formulation of conducting glue in supercapacitors. *Polymers*, 11(10):1648, 2019.

[19] Ma, C., Xie, F., Wei, L., Zheng, C., Liu, X., Wang, L. and Liu, P. All-starch-based hydrogel for flexible electronics: strain-sensitive batteries and self-powered sensors. *ACS Sustainable Chemistry & Engineering*, 10(20):6724-6735, 2022.

[20] Lu, L., Huang, Z., Li, X., Li, X., Cui, B., Yuan, C., Guo, L., Liu, P. and Dai, Q. A high-conductive, anti-freezing, antibacterial and anti-swelling starch-based physical hydrogel for multifunctional flexible wearable sensors. *International Journal of Biological Macromolecules*, 213:791-803, 2022.

[21] Railanmaa, A., Lehtimäki, S. and Lupo, D. Comparison of starch and gelatin hydrogels for non-toxic supercapacitor electrolytes. *Applied Physics A*, 123:1-8, 2017.

[22] Willfahrt, A., Steiner, E., Hötzel, J. and Crispin, X. Printable acid-modified corn starch as non-toxic, disposable hydrogel-polymer electrolyte in supercapacitors. *Applied Physics A*, 125(7):474, 2019.

[23] Morales, D., Palleau, E., Dickey, M.D. and Velev, O.D. Electro-actuated hydrogel walkers with dual responsive legs. *Soft matter*, 10(9):1337-1348, 2014.

[24] Zolfagharian, A., Kouzani, A.Z., Khoo, S.Y., Nasri-Nasrabadi, B. and Kaynak, A. Development and analysis of a 3D printed hydrogel soft actuator. *Sensors and Actuators A: Physical*, 265:94-101, 2017.

[25] Jiang, H., Fan, L., Yan, S., Li, F., Li, H. and Tang, J. Tough and electro-responsive hydrogel actuators with bidirectional bending behavior. *Nanoscale*, 11(5):2231-2237, 2019.

[26] Rotjanasuworapong, K., Thummarungsan, N., Lerdwijitjarud, W. and Sirivat, A. Facile formation of agarose hydrogel and electromechanical responses as electro-responsive hydrogel materials in actuator applications. *Carbohydrate polymers*, 247:116709, 2020.

[27] Li, Y., Sun, Y., Xiao, Y., Gao, G., Liu, S., Zhang, J. and Fu, J. Electric field actuation of tough electroactive hydrogels cross-linked by functional triblock

copolymer micelles. *ACS Applied Materials & Interfaces*, 8(39):26326-26331, 2016.

[28] Kougkolos, G., Golzio, M., Laudebat, L., Valdez-Nava, Z. and Flahaut, E. Hydrogels with electrically conductive nanomaterials for biomedical applications. *Journal of Materials Chemistry B*, 11(10):2036-2062, 2023.

[29] Lin, J., Tang, Q., Hu, D., Sun, X., Li, Q. and Wu, J. Electric field sensitivity of conducting hydrogels with interpenetrating polymer network structure. *Colloids and Surfaces A: Physicochemical and Engineering Aspects*, 346(1-3):177-183, 2009.

[30] Santaniello, T., Migliorini, L., Locatelli, E., Monaco, I., Yan, Y., Lenardi, C., Franchini, M.C. and Milani, P. Hybrid nanocomposites based on electroactive hydrogels and cellulose nanocrystals for high-sensitivity electro–mechanical underwater actuation. *Smart Materials and Structures*, 26(8):085030, 2017.

[31] Na, H., Kang, Y.W., Park, C.S., Jung, S., Kim, H.Y. and Sun, J.Y. Hydrogel-based strong and fast actuators by electroosmotic turgor pressure. *Science*, 376(6590):301-307, 2022.

[32] Jin, S., Gu, J., Shi, Y., Shao, K., Yu, X. and Yue, G. Preparation and electrical sensitive behavior of poly (N-vinylpyrrolidone-co-acrylic acid) hydrogel with flexible chain nature. *European polymer journal*, 49(7):1871-1880, 2013.

[33] Yang, C., Liu, Z., Chen, C., Shi, K., Zhang, L., Ju, X.J., Wang, W., Xie, R. and Chu, L.Y. Reduced graphene oxide-containing smart hydrogels with excellent electro-response and mechanical properties for soft actuators. *ACS applied materials & interfaces*, 9(18):15758-15767, 2017.

[34] Han, D., Farino, C., Yang, C., Scott, T., Browe, D., Choi, W., Freeman, J.W. and Lee, H. Soft robotic manipulation and locomotion with a 3D printed electroactive hydrogel. *ACS applied materials & interfaces*, 10(21):17512-17518, 2018.

[35] Wang, W., Liu, S., Yu, M. and Chen, X. Rapid 3D printing of electro-active hydrogels. *Manufacturing Letters*, 41:862-867, 2024.